














ORIGINAL RESEARCH

Wearable Seismocardiography-Based Assessment of Stroke Volume in Congenital Heart Disease

Venu G. Ganti , PhD; Asim H. Gazi , BS; Sungtae An , MS; Adith V. Srivatsa , BS; Brandi N. Nevius , MS; Christopher J. Nichols , BS; Andrew M. Carek , PhD; Munes Fares , MD; Mubeena Abdulkarim , MD; Tarique Hussain, MD, PhD; F. Gerald Greil , MD, PhD; Mozziyar Etemadi , MD, PhD; Omer T. Inan , PhD; Animesh Tandon , MD, MS

BACKGROUND: Patients with congenital heart disease (CHD) are at risk for the development of low cardiac output and other physiologic derangements, which could be detected early through continuous stroke volume (SV) measurement. Unfortunately, existing SV measurement methods are limited in the clinic because of their invasiveness (eg, thermodilution), location (eg, cardiac magnetic resonance imaging), or unreliability (eg, bioimpedance). Multimodal wearable sensing, leveraging the seismocardiogram, a sternal vibration signal associated with cardiomechanical activity, offers a means to monitoring SV conveniently, affordably, and continuously. However, it has not been evaluated in a population with significant anatomical and physiological differences (ie, children with CHD) or compared against a true gold standard (ie, cardiac magnetic resonance). Here, we present the feasibility of wearable estimation of SV in a diverse CHD population (N=45 patients).

METHODS AND RESULTS: We used our chest-worn wearable biosensor to measure baseline ECG and seismocardiogram signals from patients with CHD before and after their routine cardiovascular magnetic resonance imaging, and derived features from the measured signals, predominantly systolic time intervals, to estimate SV using ridge regression. Wearable signal features achieved acceptable SV estimation (28% error with respect to cardiovascular magnetic resonance imaging) in a held-out test set, per cardiac output measurement guidelines, with a root-mean-square error of 11.48 mL and R^2 of 0.76. Additionally, we observed that using a combination of electrical and cardiomechanical features surpassed the performance of either modality alone.

CONCLUSIONS: A convenient wearable biosensor that estimates SV enables remote monitoring of cardiac function and may potentially help identify decompensation in patients with CHD.

Key Words: cardiac output ■ machine learning ■ multimodal ■ noninvasive ■ pediatrics

Congenital heart disease (CHD) affects approximately 40000 births per year in the United States alone, a quarter of whom suffer from critical cases that require surgery or other interventions in the first year of life. Even more disturbingly, only 69% of those presenting with these critical types of CHD reach adulthood.^{1,2} Although advancements in cardiac care and surgery have significantly improved the CHD survival rate from

a few decades ago, these treatments are not curative by nature. Hence, the growing population of patients with CHD are at high risk of clinical deterioration, either sudden or gradual. Specifically, low cardiac output syndrome is the leading cause of post-CHD surgery death, whereas the development of heart failure is the leading cause of mortality among adult patients with CHD.^{3,4} Fortunately, routine assessment of key hemodynamic

Correspondence to: Venu G. Ganti, PhD, Bioengineering Graduate Program, Georgia Institute of Technology, 85 5th St NW, Atlanta, GA 30308.
Email: venu9508@gmail.com

Supplemental Material is available at <https://www.ahajournals.org/doi/suppl/10.1161/JAHA.122.026067>

For Sources of Funding and Disclosures, see page 10.

© 2022 The Authors. Published on behalf of the American Heart Association, Inc., by Wiley. This is an open access article under the terms of the [Creative Commons Attribution-NonCommercial-NoDerivs](https://creativecommons.org/licenses/by-nc-nd/4.0/) License, which permits use and distribution in any medium, provided the original work is properly cited, the use is non-commercial and no modifications or adaptations are made.

JAHA is available at: www.ahajournals.org/journal/jaha

CLINICAL PERSPECTIVE

What Is New?

- All current noninvasive stroke volume monitoring methods are inconvenient, noncontinuous, and/or expensive.
- Convenient wearable seismocardiogram and ECG sensing can estimate stroke volume, enabling longitudinal, affordable, and remote monitoring for patients with congenital heart disease.

What Are the Clinical Implications?

- In this first study of seismocardiography in patients with congenital heart disease, seismocardiogram and ECG metrics from a chest-worn wearable biosensor correlate well to stroke volume, but further longitudinal studies in larger and more diverse populations and multiple settings are needed for seismocardiography to realize its potential as a continuous, noninvasive tracker of stroke volume for those with congenital and functional heart disease.

Nonstandard Abbreviations and Acronyms

HR	heart rate
NICCOM	noninvasive continuous cardiac output monitor
PEP	pre-ejection period
RMSE	root-mean-square error
SV	stroke volume
VET	ventricular ejection time

parameters, such as ejection fraction, stroke volume (SV), and cardiac output, which is the percentage and volume of blood pumped out by the heart per heartbeat and volume per minute, has been shown to inform prognosis and guide interventions, reducing overall mortality.⁵ Because these parameters assess the ability of the heart to pump blood effectively to meet oxygen demand, they are hallmark indicators of left ventricular dysfunction⁶ when depressed and a strong predictor of major adverse cardiac events.⁷ Thus, the development of technologies allowing continuous, noninvasive, and inexpensive measurement of SV and cardiac output represents a critical need in CHD; such technologies could be used in both inpatient and outpatient settings to improve outcomes.

Existing SV and cardiac output measurement methods are suboptimal, especially in children and those with CHD. Thermodilution-based pulmonary artery catheterization is accurate, but is not commonly used in children because of the large size of catheters and

inaccuracies in patients with shunts.⁸ Transesophageal Doppler echocardiography is less invasive but cannot often be used continuously, angle dependent and therefore less accurate, bulky, and requires a trained professional.⁹ Cardiovascular magnetic resonance imaging (CMR), a noninvasive technique widely considered as the gold standard in children and those with CHD because of high accuracy and excellent reproducibility,¹⁰ is not feasible for continuous SV monitoring because of the inability to be performed at bedside or in the outpatient setting. Therefore, noninvasive continuous cardiac output monitoring (NICCOM) technologies have been developed that estimate SV from models using demographic information combined with either the impedance cardiogram or the finger arterial pressure waveform, obtained through bioimpedance and the vascular unloading technique, respectively.^{9,11} However, these approaches are obtrusive, require strict placement of multiple electrodes or cuff sizes, have low accuracy in critically ill patients, and are rarely tested in children, so their practicality remains in doubt when used for monitoring SV in patients with CHD.¹¹

Seismocardiography is a promising method for NICCOM that uses a low-noise accelerometer placed on the chest to capture the seismocardiogram, which provides cardiomechanical information unobtainable by other NICCOM methods. When combined with the ECG, the seismocardiogram allows for the calculation of systolic time intervals, such as the pre-ejection period (PEP) and ventricular ejection time (VET). In recent years, groups have demonstrated that ECG and seismocardiogram signals acquired from wearable devices can accurately estimate SV,¹² heart failure clinical status,^{13,14} and underlying events in the cardiac cycle using echocardiography and CMR¹⁵ in people with structurally normal hearts. However, seismocardiogram signals have not been evaluated in patients with CHD, resulting in a lack of understanding in how major anatomical and physiological differences, such as those present in single-ventricle patients, affect the waveform morphology. Furthermore, the ability of baseline seismocardiogram features to accurately assess diagnostic differences in absolute SV across different people has not been examined. Finally, seismocardiogram-based SV estimation has only been studied in comparison with the transesophageal Doppler echocardiogram and therefore never with respect to an unequivocal gold-standard measurement such as CMR.

We sought to evaluate the use of seismocardiography to measure SV in a unique population of patients with CHD using our convenient wearable biosensor. In this exploratory work, simple, intuitive, physiologically inspired ECG and seismocardiogram features derived from this wearable biosensor were used, along with machine learning, to estimate the baseline SV of patients with CHD undergoing clinically indicated CMR. In

addition, this preliminary work provides greater insight into how cardiomechanical signals, such as the seismocardiogram, are modulated in patients with CHD with severe anatomical and physiological differences. Ultimately, it will yield a framework, along with the pertinent features necessary, for estimating SV using wearable ECG and seismocardiogram signals toward noninvasive, continuous, and ubiquitous monitoring of this vital hemodynamic parameter.

METHODS

The data presented in this study are available from the corresponding author upon reasonable request.

Study Protocol

Detailed overviews of the study design and patient demographics are provided in [Figure 1](#) and [Table 1](#), respectively. This study was conducted under institutional review board protocol STU2019-1280 at the University of Texas Southwestern Medical Center. We approached consecutive patients with CHD undergoing clinically indicated CMR and obtained written consent and assent

as appropriate. In the preoperative area, chest-worn biosensor data were collected in a supine position for 3 minutes, unless unable to do so because of COVID-19–related anesthesia restrictions. If the patient was undergoing the scan under anesthesia, the device was placed 10 minutes after induction of anesthesia to allow for them to reach physiological equilibrium.¹⁶ During the clinical CMR scan, left ventricular and right ventricular SV, and if recommended, aortic valve forward flow, were collected per clinical protocols.¹⁷ After the CMR scan, we obtained another 3 minutes of chest-worn biosensor data, although because of space restrictions, most of these data were obtained in a sitting position. To maintain consistency with body positioning, only either pre-CMR or post-CMR supine data were examined in this work, with most data taken from the pre-CMR measurement, unless unavailable. Therefore, the similarity between pre-CMR and post-CMR measurements was not analyzed. Furthermore, matching the supine posture also used during CMR allowed us to account for the known impacts that changes in venous return because of posture can have on both SV and wearable biosignals. The aortic forward flow measurement was prioritized over the volumetric one, if acquired.

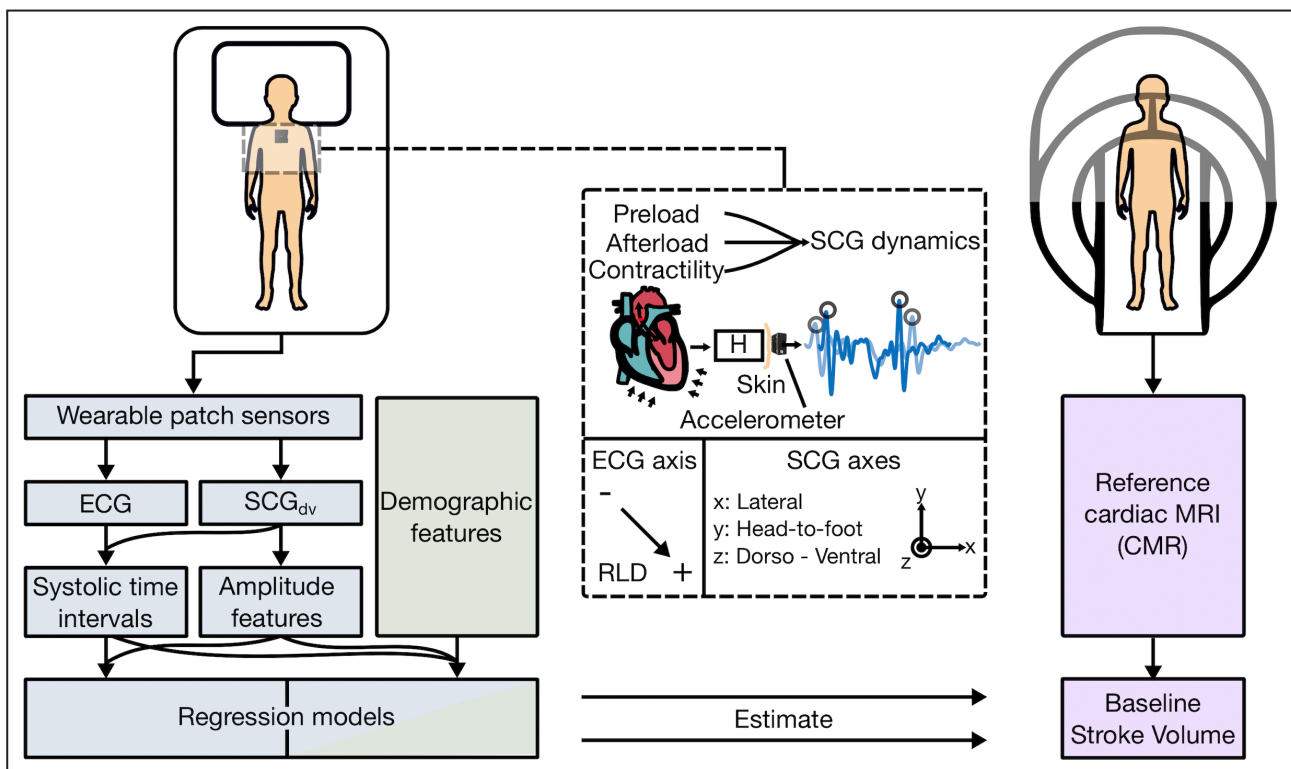


Figure 1. Concept overview.

Study design showing wearable biosensor placement when supine and asynchronous reference cardiovascular magnetic resonance imaging (CMR) measurement. Seismocardiogram (SCG) mechanistic overview detailing modulation due to cardiac physiology, acquisition with an accelerometer, and sensing axes for ECG (negative, positive, and right-leg-drive [RLD] electrodes), and triaxial SCG signals. Analysis pipeline, from sensor input to model estimation of stroke volume, for wearable (blue), demographic (green), and CMR (purple) data. H indicates the transfer function between the input internal sources of cardiomechanical vibration and the output SCG waveform measured on the surface of the torso; MRI, magnetic resonance imaging; and SCG_{dv}, dorso-ventral SCG.

Table 1. Overview of Patient Demographics and Cardiovascular Function Clinical Parameters for Study Participants

Demographics and clinical parameters	Training set, n=36	Held-out test set, n=9	P value
Sex, n (%)			1.00*
Men	22 (61)	6 (67)	
Women	14 (39)	3 (33)	
Height, cm, mean (SD)	151.3 (26.6)	163.1 (16.0)	0.21†
Weight, kg, mean (SD)	56.3 (26.0)	59.2 (19.7)	0.76†
Body surface area, m ² , mean (SD)	1.52 (0.48)	1.63 (0.34)	0.52†
Age, y, mean (SD)	15.0 (7.9)	14.7 (2.6)	0.90†
Stroke volume,‡ mL, mean (SD)	68.8 (32.34)	78.19 (24.81)	0.42†
Cardiac output,‡ L/min, mean (SD)	4.94 (1.88)	5.01 (0.84)	0.92†
Ejection fraction,‡ %, mean (SD)	0.57 (0.08)	0.59 (0.12)	0.51†
Reference heart rate, bpm, mean (SD)	76.1 (14.2)	67.7 (14.8)	0.12†
Single ventricle, n (%)	5 (14)	3 (33)	0.33*
Systemic ventricle, n (%)			0.65*
Right ventricle	6 (17)	2 (22)	
Left ventricle	30 (83)	7 (78)	

*Statistical significance between training and testing sets in categorical variables, where applicable, was computed using Fisher exact test.

†Statistical significance between training and testing sets in values, where applicable, was computed using an unpaired *t* test.

‡Values for systemic ventricle data are shown.

The systemic ventricle, which is connected to the aorta and responsible for cardiac output, was labeled by the cardiologist, and SV data from this ventricle along with the instantaneous heart rate (HR) taken from the corresponding CMR measurement, for either the volumetric or aortic forward flow measurement, were used as the reference SV and HR measurement, respectively. The systemic ventricle measurements were used for the target SV based on the assumption that features from the wearable signals would correspond more closely with the systemic ventricle responsible for ejecting the systemic SV. Additionally, patients were not separated by ventricular morphology to train ventricle-specific SV estimation models because of an already small sample size for ridge regression models and literature that suggests that SV estimates are not based on differences in systemic ventricles.¹⁸

Multimodal Hardware Design

The electronic hardware used in this study, shown in Figure 2, is an updated and miniaturized version to that previously described in detail.¹⁹ Updates focused on decreasing the overall device size to accommodate a pediatric population. From a sensing standpoint, identical

sensors and analog front ends were used in this study to acquire the ECG (ADS1291; Texas Instruments, Dallas, TX) and seismocardiogram (ADXL355; Analog Devices, Norwood, MA) signals across all versions of the hardware, and the same 3-dimensional printing filament, polylactic acid, was used to manufacture the device housing. Data were saved locally on an internal secure digital card and downloaded over universal serial bus using the custom software application previously mentioned.¹⁹ Further descriptions of the hardware used are provided in Data S1.

Signal Processing

A signal processing block diagram is depicted in Figure S1. Preprocessing consisted of bandpass filtering the ECG and the dorso-ventral axis of the seismocardiogram signal between 5 and 30 Hz, and 0.8 and 30 Hz to remove their respective out-of-band noise. The seismocardiogram was also filtered into a higher frequency bandwidth 30 to 125 Hz to produce a signal hereafter referred to as high-frequency seismocardiogram, which is more closely representative of the phonocardiogram. In turn, this wider bandwidth accelerometer signal is capable of picking up on higher frequency vibrations, coupled to the acoustics of the phonocardiogram, thus offering a more reliable timeframe to estimate aortic valve opening and closing events,²⁰ a common technical challenge in seismocardiogram processing.¹⁹ After filtering, all signals were resampled to 1 kHz. The R peaks of the ECG were used to segment the seismocardiogram and high-frequency seismocardiogram signals into different heartbeats. The seismocardiogram and high-frequency seismocardiogram heartbeats were ensemble averaged using 30 heartbeat windows with 50% overlap to reduce 0 mean noise, account for respiratory-induced variability in seismocardiogram signals, and improve the consistency of amplitude features before selecting the highest signal-to-noise ratio beat later used to extract the features shown in Table 2. A detailed description of the calculation and meaning of the features used is provided in Data S1.

Machine-Learning Regression Analysis

Ridge regression was used to estimate SV because of its ability to handle multicollinearity, a trait common among systolic time intervals, as well as provide feature importance with reduced complexity simply from its weights as a linear model. To avoid data leakage, an 80% to 20% fixed training-testing scheme (ie, 36 patients for training, 9 for testing) was determined using a true random number generator (RANDOM.ORG, Dublin, Ireland). A 10-fold cross-validation on the training set was used to perform the grid search necessary for hyperparameter optimization. Forward feature selection, on the training set, was used to reduce the feature set from 14 down to 9 features by examining the coefficient

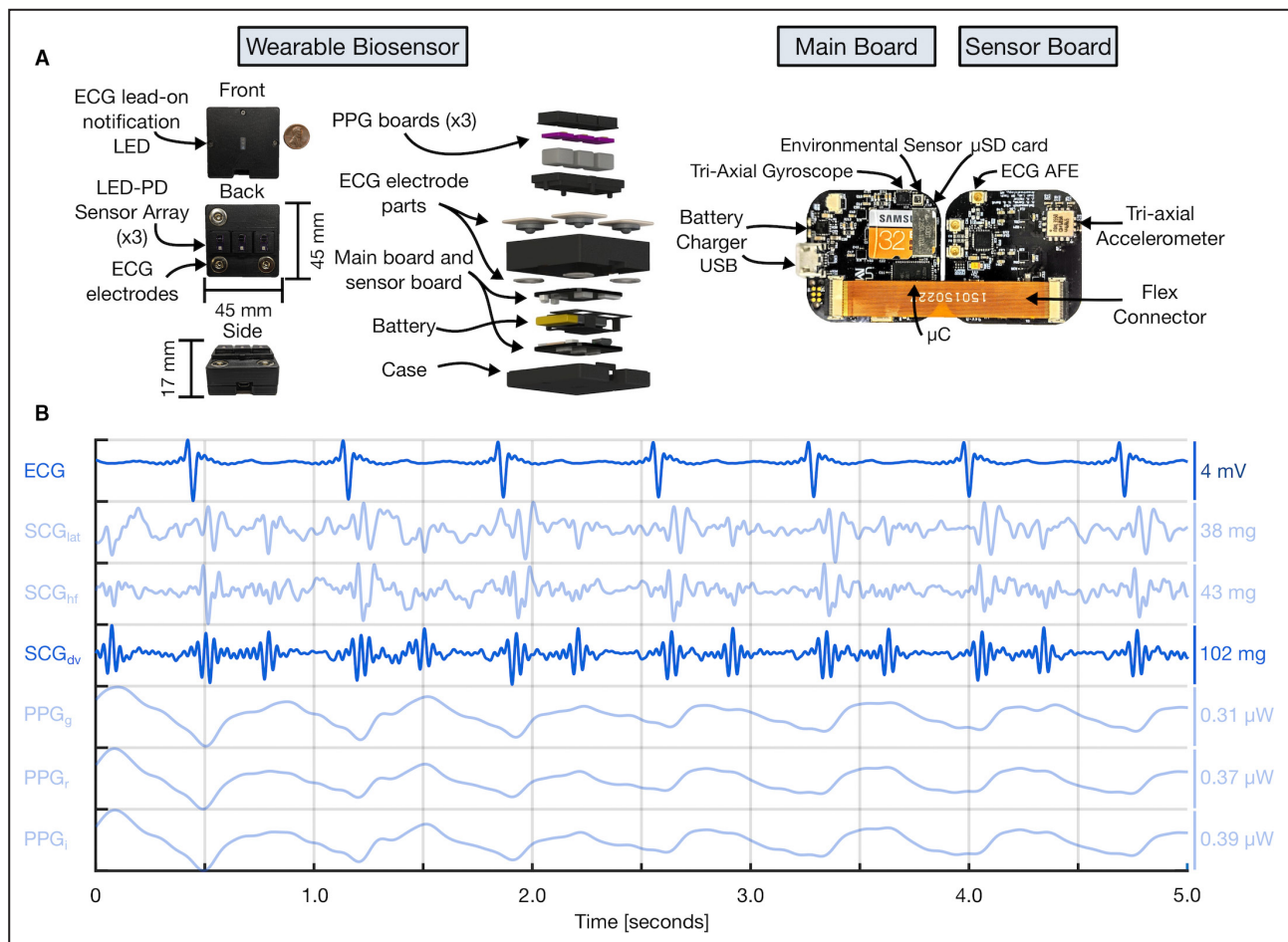


Figure 2. Wearable multimodal hardware engineering mechanics.

A, Pertinent multimodal hardware diagram. Final wearable biosensor iteration with exploded view detailing photoplethysmogram (PPG) components, gel-electrode ECG connectors, lithium-polymer battery, and printed circuit boards (PCBs). Main PCB with ATSAM4LS8 microcontroller (μC), BMG250 triaxial gyroscope and BME280 environmental sensor, micro secure digital card (μSD), and BQ24232 battery charger. Sensor PCB, connected to main PCB via flexible connector, with ADXL355 accelerometer, ADS1291 analog front end, and magnetic wire connections to separate PCB containing SFH7016 multichip light-emitting diode (LED) and SFH 2703 photodiode (PD) used to acquire triaxial seismocardiogram (SCG), single-lead ECG, and multiwavelength sternum PPG signals, respectively. **B**, Sample 5 seconds of filtered wearable signal data from a single-ventricle patient with corresponding amplitudes are shown. In order from top to bottom: ECG, lateral SCG (SCG_{lat}), head-to-foot SCG (SCG_{ht}), dorso-ventral SCG (SCG_{dv}), green PPG (PPG_g), red PPG (PPG_r), and infrared PPG (PPG_i) signals. The darker blue ECG and SCG_{dv} signals are those used in this work. USB indicates universal serial bus.

of determination, through simple linear regression between ECG and seismocardiogram features and SV. Different ridge regression models, trained on a combination of feature sets, each with their respective optimized λ hyperparameter from the 10-fold cross-validation on the training set, were used to estimate SV. Specifically, we began by examining a model that was merely trained on demographic features alone (ie, body surface area and age) because of their well-known correlation to cardiac output,²¹ which assessed the ability to quantify SV without the use of a wearable biosensor. Next, we tested using ECG features, namely HR, to assess the estimation accuracy when using only a conventional metric that is readily, remotely, and continuously available through Holter monitors. Then, we tested our novel approach by

adding seismocardiogram features to the ECG model to provide for a holistic evaluation of both the electrical and mechanical aspects of cardiac health. Finally, we have provided various combinations of these wearable biosensor and demographic feature sets to determine whether the easily accessible demographic information can augment model estimation.

Statistical Analysis

To assess these model performances, we computed the root-mean-square error (RMSE) and the coefficient of determination (R^2) between the estimated SV and true CMR SV in the held-out test set that was unseen to the machine-learning algorithm until final testing. Percent error was calculated for the highest performing

Table 2. Physiological Features and Corresponding Measurement System

Feature name	Measurement system
Heart rate	Both reference CMR and wearable system
PEP	Wearable system
VET	Wearable system
Timing of AC	Wearable system
Root-mean-square power during PEP	Wearable system
Root-mean-square power during VET	Wearable system
PEP-to-VET ratio	Wearable system
VET-to-PEP ratio	Wearable system

AC indicates aortic valve closure; CMR, cardiovascular magnetic resonance imaging; PEP, pre-ejection period; and VET, ventricular ejection time.

model given the guidelines for cardiac output measurement devices as the limits of agreement (ie, 1.96 times the SD of the bias) divided by the mean SV from the CMR and wearable $\times 100$, with a percent error $<30\%$ regarded as acceptable.²² Importance of the features was derived from the magnitude of the weights from ridge regression, and importance of the permutations, iterated 1000 times, were also computed and are provided in Figure S2. Specifics on model selection, train-test splitting, cross-validation, and feature selection are provided in Data S1.

RESULTS

We enrolled 57 patients and successfully acquired both supine wearable and CMR data from 45 patients. Twelve patients were excluded because they either did not contain accompanying CMR, a supine wearable measurement because of COVID-19 anesthesia area restrictions, usable wearable data because of system malfunction, or withdrew from the study. Their detailed patient demographics are presented in Table 1. The regression model performance, the coefficient of

Table 3. Ridge Regression Performance Using Different Feature Sets

Feature set	10-fold CV training set, R^2	Held-out test set, R^2	RMSE, mL
ECG	0.47	0.69	13.05
SCG	0.22	0.23	20.51
Age+BSA	0.72	-0.10	24.56
ECG+SCG	0.49	0.76	11.48
ECG+SCG+Age+BSA	0.88	0.27	19.94
ECG+SCG+BSA	0.74	0.46	17.20

BSA indicates body surface area; CV, cross-validation; RMSE, root-mean-square error; and SCG, seismocardiogram.

determination and RMSE, for the training (ie, 10-fold CV) and testing set for all feature sets is shown in Table 3.

The test set performance, when combining features from both the ECG and seismocardiogram modalities, improved upon that of the ECG model alone (R^2 , 0.76 and RMSE, 11.48 mL versus R^2 , 0.69 and RMSE, 13.05 mL) and substantially upon the demographic one (R^2 , -0.10 and RMSE, 24.56 mL). However, the ECG-only model still outperformed the seismocardiogram only model (R^2 , 0.20 and RMSE, 20.51 mL). To put the significance of these low RMSEs into context, the dynamic range of measured SV in the training and test set were 146.5 and 74.8 mL, respectively. The regression and Bland-Altman plot for the highest performing model, combining ECG and seismocardiogram features to estimate SV, are shown in Figure 3. The 95% CIs for the highest performing model train and test sets are -44.63 to 44.63 mL and -23.82 to 20.8 mL, respectively. The percent error, the metric that is used by cardiac output measurement guidelines, for this highest performing model was 28%, within the acceptable criteria of 30%.²² By contrast, the percent error for the ECG-only model was outside the threshold for acceptability at 31%.

The demographic feature model has a stark difference between training (R^2 , 0.72) and testing (R^2 , -0.10) performance, a clear sign of overfitting. Therefore, combining the demographic information with ECG and seismocardiogram features improved their training set performance (R^2 , 0.88), but not the test set performance (R^2 , 0.27). However, as presented in Table 1, there was no significant difference between the demographics of the training and testing set.

The importance of the features based on the magnitude of the weights from the ridge regression model is shown in Figure 4. Other than HR, the most important features are either the PEP, VET, or a ratio derived from the combination of them. The importance of the permutations, given in Figure S2, was comparable to the magnitude of the weights from ridge regression, but with VET and PEP having opposite ordering in importance. In addition, the Pearson correlation coefficients between the physiological features and SV, provided in Table S1, demonstrate that HR, aortic valve closure, and VET have the greatest correlation to SV while also giving indication of their relationship to SV.

DISCUSSION

In this preliminary study, we show that a combination of seismocardiogram and ECG parameters, obtained noninvasively, can be acceptable estimators of SV in patients with CHD undergoing CMR per cardiac output

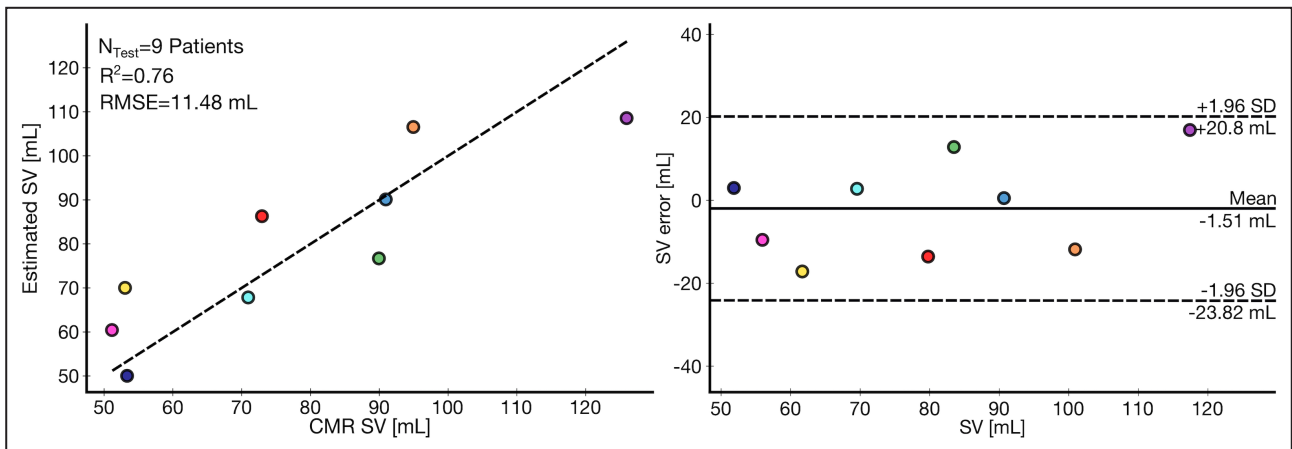


Figure 3. Wearable stroke volume (SV) estimation results.

Correlation and Bland-Altman plots between wearable signal estimated SV and the cardiovascular magnetic resonance imaging (CMR) imaging SV for held-out test set of 9 patients. The coefficient of determination (R^2 , 0.76) and root-mean-square error (RMSE, 11.48 mL) are shown.

measurement guidelines.²² This exploratory work represents a necessary advancement toward both more holistic wearable SV estimation for diagnostics and remote monitoring for patients with CHD. Furthermore, our study is novel in using seismocardiography in children and those with CHD; other studies have focused on structurally normal hearts. Specifically, although it has been shown previously that noninvasive ECG and seismocardiogram measurements contain information that can be used to estimate SV,¹² this relationship had not been examined in a diverse population of patients with congenital heart defects and compared against a true gold-standard measurement. Here, we evaluated

the future usefulness of a convenient method for estimating SV and observed that there was a strong correlation between simple, highly interpretable seismocardiogram features and SV, across a wide range of CHD diagnoses, ages, and anatomical differences. We further achieved acceptable estimation of SV in a completely held-out test set by using a regression model that combined both electrical and cardiomechanical wearable features, producing performance superior to that of either feature subset alone.

Wearable Multimodal Signal Features Are the First Acceptable Estimator of Baseline SV in a Completely Held-Out Test Set of Patients With CHD

Wearable features were strongly correlated to baseline gold-standard CMR SV in a heterogeneous population of patients with CHD. Furthermore, with an overall 28% error, we were able to achieve an acceptable estimation of SV, based on the limits set forth by cardiac output measurement guidelines, in a completely randomized held-out test set.²² Meanwhile, the training set, for which the model was an unacceptable estimator of SV based on the guidelines, had a wide dynamic range of nearly double that of the test set of 146.5 mL, which may explain the lower performance therein and the discrepancy observed in this random set. Overall, this SV estimation model trained on multimodal wearable signal features and tested on unseen data is of greater use than a purely correlation-based result. Additionally, for the Bland-Altman analysis, all estimations were within the limits of agreement indicative of high model precision. Meanwhile, existing inconvenient methods, although more comprehensively evaluated, such as transesophageal Doppler and NICCOM methods,

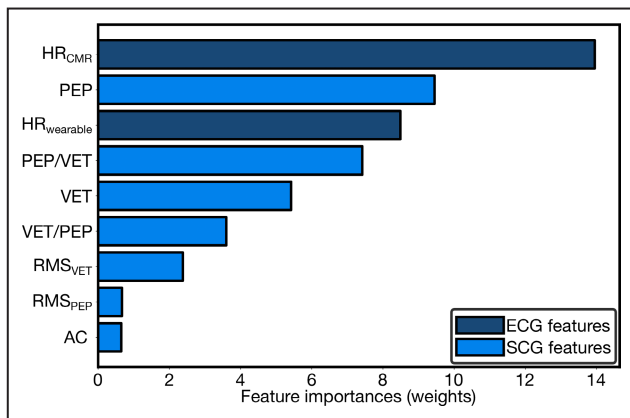


Figure 4. Importance of features for stroke volume estimation model.

Importance of features for wearable system from magnitude of ridge regression weights ranked in order from top to bottom and color-coded by wearable sensing modality, ECG and seismocardiogram (SCG) signals. AC indicates aortic valve closure; CMR, cardiovascular magnetic resonance imaging; HR, heart rate; PEP, pre-ejection period; RMS, root-mean-square; and VET, ventricular ejection time.

have estimation errors of $>40\%$.²³ In the field of physiological research and biomedical signal processing, to be able to use baseline measurements to estimate absolute values in clinical parameters across a subject population is extremely difficult and rarely performed. Typically, a perturbation or intervention is leveraged to modulate physiological properties, in this case hemodynamics, which allows for a greater dynamic range and ability to track subject-specific changes in waveform morphology, usually resulting in higher accuracy. In this study, the comprehensive age range and diagnoses, representative of higher-risk children and adults with CHD who would be undergoing CMR, not only adds difficulty in hardware design, but also contributes to high intersubject variability. Eventually, if the device were to be used to obtain continuous, noninvasive measurements, perhaps in the case of monitoring patients with CHD after surgery for low cardiac output syndrome, then tracking subject-specific changes in seismocardiogram signals would suffice to monitor status, predict exacerbation, and offer personalized health care without a specific gold-standard baseline assessment. Generally, subject-specific models will outperform globalized models, although the reduced complexity of the latter may prove to be beneficial in certain scenarios.

Our low RMSE for the test set of 11.48 mL, underscored by the wide dynamic range in SV of 74.8 mL within, demonstrates that our estimation is relatively robust to outliers. Hence, the inability to explain these outliers with a demographics-only model, which performed worse than our overall model, suggests that the acceptable estimation was not driven primarily by patient size (eg, body surface area). From the residual errors in the regression plot shown in [Figure 3](#), our model also had comparable estimation of high and low SVs: a well-known limitation of machine-learning approaches that cleverly estimate the mean to reduce error. However, there was a slightly better performance at lower SV, most likely because of a greater number of data points with similar target values. Additionally, in our training set, there were fewer data points near the highest SVs as well, which lead to the greatest error when estimating them and potentially explains the difference between the training and testing performance. Therefore, increasing the number of data points with an emphasis on those exhibiting the boundaries of SV should improve estimation performance and overall model robustness.

Nevertheless, using wearable signal features as an acceptable estimator of SV across a heterogeneous population of patients with CHD, suggests that eventually seismocardiogram signals can assist in overall diagnostics, which was previously not demonstrated in seismocardiography literature.

Cardiomechanical Seismocardiogram Features Improve Model Estimation

As shown in [Table 2](#), adding the cardiomechanical seismocardiogram features to the purely electrical ECG model resulted in a modest improvement in performance that reduced the percent error from 31% to 28%, which was sufficient to achieve acceptable SV estimation per cardiac output measurement guidelines. Although the heart is electrically activated, it remains a mechanical pump, and therefore assessing these other aspects of cardiac health, although traditionally ignored by NICCOM methods, are essential to quantifying its mechanical function. Specifically, although HR is well known to exhibit a strong correlation to SV, the other most important features essential to achieving a good estimation were the PEP, VET, and PEP/VET.^{24,25} The PEP, a combination of the intrinsic electromechanical delay and isovolumic contraction time, was our second most important feature. This is in accordance with established knowledge that the PEP can vary based on age, between infancy and puberty, and differences in contractility and preload, both captured in our data set.²⁶ Similarly, the VET, the time it takes to eject the SV of blood out the aorta, is related to SV.^{24,26} In addition, several NICCOM technologies use the impedance cardiogram to estimate SV through mathematical formulas, which are grounded in well-understood relationships between bioimpedance and cardiac output,²⁷ and leverage the VET as a strong correlate to SV. However, bioimpedance inconveniently requires multiple electrodes to be placed on the body, whereas seismocardiography can capture the same VET in a significantly more convenient manner simply through an accelerometer placed on the chest. Additionally, their ratio (ie, PEP/VET) has been demonstrated to be inversely related to contractility and helpful in determining heart failure.²⁸ This relationship is understood to be because of the greater amount of time required for the failing heart to build up the pressure necessary for ejection, related to PEP, and the smaller SV ejected during a shorter VET.²⁸

Though the ECG features had a more significant independent contribution in estimating baseline SV, the seismocardiogram signal has been shown to better capture longitudinal changes in ventricular function by assessing the mechanical aspects of cardiac health.^{12,13} Nonetheless, given the complex determinants of SV, it is not surprising that combining features from multiple sensing modalities was necessary to create the holistic model that had the greatest performance.

Demographic Based Correlations to SV Do Not Necessarily Generalize

Demographic feature models (ie, those using age and body surface area) did not generalize well to our

held-out test set. Typically, body surface area is known to be well correlated to cardiac output, especially in this population with significant age and developmental size differences.²¹ However, although these demographic feature models substantially improved training set performance, these improvements did not translate to the test set. This inability to generalize well in cases when the conventional trend between SV and demographics may not be observed,²⁹ suggests that the proper physiological data in waveform format are necessary for the robust estimation of SV. Overall, demographics may be misleading, especially in populations presenting with the unique anatomies and extreme physiologies typical to those with underlying CHD. Regardless, with an increasing number of data points, the contribution of these demographic features should be used for a similar diagnostic application. Specifically, given our SV estimation and the available wearable HR, these demographic characteristics can clearly be incorporated if the body surface area is correlated to SV, to compute cardiac index, which is commonly used in pediatric cardiology to assess adequacy of oxygen delivery.

SV Estimation Is Robust Against Anatomical Differences

Largely, our data suggest that acceptable SV estimation can be achieved regardless of the unique anatomies and physiologies in patients with CHD. Although there are considerable anatomical modifications between single-ventricle and 2-ventricle patients, it has previously been shown that there are no distinguishable differences in their SV estimation before and after the hemi-Fontan operation when using magnetic resonance imaging.¹⁸ In addition, because of their wide-ranging diagnoses and demographics, the intersubject variability in the single-ventricle patients may have overshadowed their population variability with respect to the 2-ventricle patients. In future studies, to fully determine whether any anatomically induced modulation in seismocardiogram morphology exists, data should be taken from a larger and more homogenous single-ventricle population, for instance, reducing the age gap to only neonates with single and 2 ventricles.

Eventually, remote monitoring of the growing population of older children and adults with heart defects appears to be more feasible because of their uncoupled characteristics with respect to this novel sensing modality and key hemodynamic parameters of ventricular function such as SV.

Future Work

In this novel, exploratory work relating wearable signals to SV in patients with CHD, we present technology that can be refined to improve accuracy through

multiple means from developments in the wearable device, data collection, and algorithms used herein. Specifically, plethysmogram signals were not used in this work; however, features from the plethysmogram have been shown to be correlated to SV and offer a measure of peripheral hemodynamics that is uncaptured by the seismocardiogram and ECG.³⁰ This alternative modality when fused with the seismocardiogram and ECG can likely help improve performance by creating a more holistic model. Next, when using machine-learning methods, increasing data size can have significant influence on determining true model accuracy and generalizability. Therefore, further studies should aim to collect data on more patients with similar diagnoses for longer periods of time, perhaps with a continuous SV reference measurement, and analyze differences between either single- and 2-ventricle patients or those with a systemic right versus systemic left ventricle, separately. Using longitudinal data to train subject-specific models will likely result in increased accuracy when compared with non-subject-specific models. Finally, with an increase in data from both another modality measured by the device and sample size, more complex machine-learning algorithms can be used to better estimate SV.

STUDY LIMITATIONS

This study has limitations related to both the technologies used and the patient population studied. The wearable biosensor is not magnetic resonance imaging safe, and thus, simultaneous measurement of CMR flows and volumetrics with ECG and seismocardiogram was not possible. Thus, to mitigate this limitation, we obtained the wearable measurements as soon as possible before and after the CMR scan and after the patient was under anesthesia for those getting the CMR with anesthesia. However, it is possible that the patients were in different physiologic states during the CMR compared with when the wearable measurements were taken. Furthermore, the small population studied herein, especially considering the application of machine learning to estimate SV, requires the model to be further validated in patients with CHD to ensure generalizability. To mitigate this in this first study, we used a small subset of highly interpretable features along with a ridge regression model that offers a regularization penalty to reduce model overfitting and used a fixed train-test split. Regardless, this study represents exploratory work, because the accuracy of machine-learning models with small sample sizes cannot be truly determined until more data are collected in multiple settings. Overall seismocardiogram and ECG metrics from a chest-worn wearable biosensor correlate well to SV, but further longitudinal studies in larger

and more diverse populations and multiple settings are needed for seismocardiography to realize its potential as a continuous, noninvasive tracker of SV for those with congenital and functional heart disease.

CONCLUSIONS

We demonstrated that a multimodal wearable biosensor that measures both seismocardiogram and ECG signals can serve as an acceptable estimator of SV in patients with CHD based on the cardiac output measurement guidelines. In the future, this exploratory work could be expanded to monitor patients conveniently and longitudinally either after surgery or from the comfort of their homes. Noninvasive, continuous monitoring of SV using a wearable biosensor equips clinicians with the tools necessary to track their patients longitudinally, not currently captured by any clinical program and seldom studied, which is essential to comprehend the lifetime complications facing this growing population. Eventually, advanced machine-learning algorithms may even be capable of predicting the periodic decompensations of patients with CHD. In addition, it is well known that there are racial, socioeconomic, and geographic factors that contribute to disturbing health disparities in CHD mortality.³¹ Ultimately, following further studies in a larger population, an inexpensive ECG and seismocardiogram wearable biosensor may provide accurate low-user-input SV monitoring in a noninvasive, continuous, and affordable manner for patients in out-of-office settings in low-resource settings.

ARTICLE INFORMATION

Received March 9, 2022; accepted August 8, 2022.

Affiliations

Bioengineering Graduate Program (V.G.G., O.T.I.); School of Electrical and Computer Engineering (A.H.G., O.T.I.), School of Interactive Computing (S.A.); The Wallace H. Coulter Department of Biomedical Engineering (A.V.S., C.J.N.), and School of Mechanical Engineering (B.N.N.), Georgia Institute of Technology, Atlanta, GA; Department of Biomedical Engineering, McCormick School of Engineering (A.M.C., M.E.), and Department of Anesthesiology, Feinberg School of Medicine (A.M.C., M.E.), Northwestern University, Evanston, IL; Department of Pediatrics, University of Texas Southwestern Medical Center, Dallas, TX (M.F., M.A., T.H., F.G.G., A.T.); and Cleveland Clinic Children's, Cleveland, OH (A.T.).

Acknowledgments

The authors recognize M. Martinez and W. Anguiano for their contributions in the data collection process and J.A. Heller for his efforts in the design and review of the electronic hardware.

Sources of Funding

This work was funded by the Children's Health Innovation Fund; Children's Health, Dallas, Texas; Saving Tiny Hearts Society; Thrasher Foundation Early Career grant (all to A.T.). A.H.G. was supported by a National Science Foundation Graduate Research Fellowship (DGE-2039655).

Disclosures

Dr Inan is a cofounder, board member, and chief scientific advisor to Cardiosense, and a scientific advisor for Physiowave. Dr Etemadi is a

cofounder, board member, and scientific advisor to Cardiosense. Dr Carek is a cofounder and chief technology officer of Cardiosense. Dr Tandon has significant grant funding from Synergen Technologies. The funders had no role in the design of the study; in the collection, analyses, or interpretation of data; in the writing of the article; or in the decision to publish the results. The remaining authors have no disclosures to report.

Supplemental Material

Appendix S1
Table S1
Figures S1–S2
References [32–35]

REFERENCES

- Hoffman JLE, Kaplan S. The incidence of congenital heart disease. *J Am Coll Cardiol*. 2002;39:1890–1900. doi: 10.1016/S0735-1097(02)01886-7
- Oster ME, Lee KA, Honein MA, Riehle-Colarusso T, Shin M, Correa A. Temporal trends in survival among infants with critical congenital heart defects. *Pediatrics*. 2013;131:e1502–e1508. doi: 10.1542/peds.2012-3435
- Ma M, Gauvreau K, Allan CK, Mayer JE Jr, Jenkins KJ. Causes of death after congenital heart surgery. *Ann Thorac Surg*. 2007;83:1438–1445. doi: 10.1016/j.athoracsur.2006.10.073
- Burchill LJ, Gao L, Kovacs AH, Opatowsky AR, Maxwell BG, Minnier J, Khan AM, Broberg CS. Hospitalization trends and health resource use for adult congenital heart disease-related heart failure. *J Am Heart Assoc*. 2018;7. doi: 10.1161/JAHA.118.008775
- Klem I, Shah DJ, White RD, Pennell DJ, van Rossum AC, Regenfus M, Sechtem U, Schwartzman PR, Hunold P, Croisille P, et al. Prognostic value of routine cardiac magnetic resonance assessment of left ventricular ejection fraction and myocardial damage. *Circ Cardiovasc Imaging*. 2011;4:610–619. doi: 10.1161/CIRCIMAGING.111.964965
- Abuhsaud AO, Lowe BS, Guo K, Marelli AJ, Kaouache M, Guo L, Jutras L, Martucci G, Therrien J. Cardiac output as a predictor in congenital heart disease: Are we stating the obvious? *Int J Cardiol*. 2016;210:143–148. doi: 10.1016/j.ijcard.2016.02.071
- Valente AM, Gauvreau K, Assenza GE, Babu-Narayan SV, Schreiber J, Gatzoulis MA, Groenink M, Inuzuka R, Kilner PJ, Koyak Z, et al. Contemporary predictors of death and sustained ventricular tachycardia in patients with repaired tetralogy of Fallot enrolled in the INDICATOR cohort. *Heart*. 2014;100:247–253. doi: 10.1136/heartjnl-2013-304958
- Connors AF, Speroff T, Dawson NV, Thomas C, Harrell FE, Wagner D, Desbiens N, Goldman L, Wu AW, Califf RM, et al. The effectiveness of right heart catheterization in the initial care of critically ill patients. *J Am Med Assoc*. 1996;276:889–897. doi: 10.1001/jama.1996.03540110043030
- Kerstens MK, Wijnberge M, Geerts BF, Vlaar AP, Veelo DP. Non-invasive cardiac output monitoring techniques in the ICU. *Neth J Crit Care*. 2018;26:104–110. Available at: <http://www.deltexmedical.com/downloads/clinicaleducationguides>
- Grothues F, Smith GC, Moon JCC, Bellenger NG, Collins P, Klein HU, Pennell DJ. Comparison of interstudy reproducibility of cardiovascular magnetic resonance with two-dimensional echocardiography in normal subjects and in patients with heart failure or left ventricular hypertrophy. *Am J Cardiol*. 2002;90:29–34. doi: 10.1016/S0002-9149(02)02381-0
- Saugel B, Cecconi M, Wagner JY, Reuter DA. Noninvasive continuous cardiac output monitoring in perioperative and intensive care medicine. *Br J Anaesth*. 2015;114:562–575. doi: 10.1093/bja/aeu447
- Semiz B, Carek AM, Johnson JC, Ahmad S, Heller JA, Garcia-Vicente FG, Caron S, Hogue CW, Etemadi M, Inan O. Non-invasive wearable patch utilizing seismocardiography for peri-operative use in surgical patients. *IEEE J Biomed Heal Informatics*. 2021;25:1572–1582. doi: 10.1109/JBHI.2020.3032938
- Inan OT, Baran Pouyan M, Javaid AQ, Dowling S, Etemadi M, Dorier A, Heller JA, Bicen AO, Roy S, De Marco T, et al. Novel wearable seismocardiography and machine learning algorithms can assess clinical status of heart failure patients. *Circ Heart Fail*. 2018;11:e004313. doi: 10.1161/CIRCHEARTFAILURE.117.004313
- Herkert C, Migeotte PF, Hossein A, Spee RF, Kemps HMC. The kinocardiograph for assessment of changes in haemodynamic load in patients with chronic heart failure with reduced ejection fraction. *ESC Heart Fail*. 2021;8:4925–4932. doi: 10.1002/ehf2.13522

15. Akhbardeh A, Tavakolian K, Gurev V, Lee T, New W, Kaminska B, Trayanova N. Comparative analysis of three different modalities for characterization of the seismocardiogram. *Annu Int Conf IEEE Eng Med Biol Soc.* 2009;2899–2903. doi: 10.1109/IEMBS.2009.5334444
16. Taylor K, Manlihot C, McCrindle B, Grosse-Wortmann L, Holtby H. Poor accuracy of noninvasive cardiac output monitoring using bioimpedance cardiography [PhysioFlow®] compared to magnetic resonance imaging in pediatric patients. *Anesth Analg.* 2012;114:771–775. doi: 10.1213/ANE.0b013e318246c32c
17. Fratz S, Chung T, Greil GF, Samyn MM, Taylor AM, Valsangiacomo Buechel ER, Yoo SJ, Powell AJ. Guidelines and protocols for cardiovascular magnetic resonance in children and adults with congenital heart disease: SCMR expert consensus group on congenital heart disease. *J Cardiovasc Magn Reson.* 2013;15:1–26. doi: 10.1186/1532-429X-15-51
18. Bellsham-Revell HR, Tibby SM, Bell AJ, Witter T, Simpson J, Beerbaum P, Anderson D, Austin CB, Greil GF, Razavi R. Serial magnetic resonance imaging in hypoplastic left heart syndrome gives valuable insight into ventricular and vascular adaptation. *J Am Coll Cardiol.* 2013;61:561–570. doi: 10.1016/j.jacc.2012.11.016
19. Ganti VG, Carek A, Nevius BN, Heller J, Etemadi M, Inan O. Wearable cuff-less blood pressure estimation at home via pulse transit time. *IEEE J Biomed Heal Informatics.* 2021;25:1926–1937. doi: 10.1109/JBHI.2020.3021532
20. Carek AM, Conant J, Joshi A, Kang H, Inan OT. SeismoWatch. *Proc ACM Interactive, Mobile, Wearable Ubiquitous Technol.* 2017;1:1–16. doi: 10.1145/3130905
21. Jegier BW, Sekelj P, Auld PAM, Simpson R, McGregor M. The relation between cardiac output and body size. *Hear J first.* 1963;25:425–430. doi: 10.1136/hrt.25.4.425
22. Critchley LAH, Critchley JAJH. A meta-analysis of studies using bias and precision statistics to compare cardiac output measurement techniques. *J Clin Monit Comput.* 1999;15:85–91. doi: 10.1023/A:1009982611386
23. Peyton PJ, Chong SW. Minimally invasive measurement of cardiac output during surgery and critical care: A meta-analysis of accuracy and precision. *Anesthesiology.* 2010;113:1220–1235. doi: 10.1097/ALN.0b013e3181ee3130
24. Weissler AM, Peeler RG, Roehll WH. Relationships between left ventricular ejection time, stroke volume, and heart rate in normal individuals and patients with cardiovascular disease. *Am Heart J.* 1961;62:367–378. doi: 10.1016/0002-8703(61)90403-3
25. Winberg P, Ergander U. Relationship between heart rate, left ventricular output, and stroke volume in preterm infants during fluctuations in heart rate. *Pediatr Res.* 1992;31:117–120. doi: 10.1203/00006450-199202000-00005
26. Lewis RP, Rittgers SE, Forester WF, Boudoulas H. Reviews of contemporary laboratory methods. A Critical Review of the Systolic Time Intervals. Available at: <http://ahajournals.org>. Accessed August 5, 2021.
27. Bernstein DP, Lemmens HJM. Stroke volume equation for impedance cardiography. *Med Biol Eng Comput.* 2005;43:443–450. doi: 10.1007/BF02344724
28. Bonagura JD, Fuentes VL. Chapter 8 - Echocardiography. In: Mattoon JS, Nyland TG, eds. *Small Animal Diagnostic Ultrasound (Third Edition)*. W.B. Saunders; 2015:217–331. doi: 10.1016/B978-1-4160-4867-1.00008-8
29. Vriesendorp MD, Groenwold RHH, Herrmann HC, Head SJ, Van WRAFDL, Vriesendorp PA, Kappetein AP, RJM K. The clinical implications of body surface area as a poor proxy for cardiac output. *Structural Heart.* 2021;5:582–587. doi: 10.1080/24748706.2021.1968089
30. Yao Y, Shin S, Mousavi A, Kim C-S, Xu L, Mukkamala R, Hahn J-O. Unobtrusive estimation of cardiovascular parameters with limb ballistocardiography. *Sensors (Basel).* 2019;19:2922. doi: 10.3390/S19132922
31. Kaltman JR, Burns KM, Pearson GD, Goff DC, Evans F. Disparities in congenital heart disease mortality based on proximity to a specialized pediatric cardiac center. *Circulation.* 2020;141:1034–1036. doi: 10.1161/CIRCULATIONAHA.119.043392
32. Kim S, Leonhardt S, Zimmermann N, Kranen P, Kensche D, Müller E, Quix C. Influence of contact pressure and moisture on the signal quality of a newly developed textile ECG sensor shirt. *Proceedings of the 5th International Workshop on Wearable and Implantable Body Sensor Networks (BSN 2008) in conjunction with the 5th International Summer School and Symposium on Medical Devices and Biosensors (ISSS-MDBS 2008)*. 2008; 256–259. doi: 10.1109/ISSMDBS.2008.4575068
33. Ha T, Tran J, Liu S, Jang H, Jeong H, Mitbender R, Huh H, Qiu Y, Duong J, Wang RL, et al. A chest-laminated ultrathin and stretchable E-tattoo for the measurement of electrocardiogram, seismocardiogram, and cardiac time intervals. *Adv Sci.* 2019;6:1900290. doi: 10.1002/advs.201900290
34. Inan OT, Kovacs GTA, Giovangrandi L. Evaluating the lower-body electromyogram signal acquired from the feet as a noise reference for standing ballistocardiogram measurements. *IEEE Trans Inf Technol Biomed.* 2010;14:1188–1196. doi: 10.1109/TITB.2010.2044185
35. Sani OG, Yang Y, Lee MB, Dawes HE, Chang EF, Shانهchi MM. Mood variations decoded from multi-site intracranial human brain activity. *Nat Biotechnol.* 2018;36:954–961. doi: 10.1038/nbt.4200

Supplemental Material

Data S1

Supplemental Methods

Multimodal hardware design

Overall, the key upgrades from the hardware used in¹⁹ include the addition of a flexible connector, two main sensing printed circuit boards as opposed to three, eventually the use of gel-electrode ECG, a separate photoplethysmogram sensor board with newer discretized photodiodes and light-emitting-diodes, and a foam-based spring backing mechanism for improved photoplethysmogram sensing. However, the photoplethysmogram signals were not explored in this work and therefore—to prevent detracting from the focus of this work—the specific details of that hardware will not be expanded on further. The sample rate of the ECG was 1kHz and the SCG either 500Hz or 2kHz depending on the prototype version. Specifically, in the newer version, shown in Figure 2a, the sample rate of the SCG was increased to 2 kHz to provide a bandwidth of 500 Hz; the SCG sampling frequency was adjusted to capture higher frequency sounds that may eventually be utilized to monitor patients with heart murmurs—a subsection of the CHD population at a greater risk of decline. Unfortunately, as with a proof-of-concept study, the hardware required few—mostly device housing—modifications at different stages of the study before reaching the current prototype pictured in Figure 2a. Most importantly, the earlier version of the hardware utilized in this study featured the use of a dry electrode ECG, using stainless steel tape, for which the device was pressed against the chest of the patient to acquire the biosignals, while the later version used standard infant AgCl gel electrodes (Kendall HP69, Medtronic PLC, Dublin, Ireland) to adhere to the chest, eliminating the need for an extra contact force. To help mitigate any issues from differences in contact pressure with the dry electrode

version, in addition to having the same group of few clinicians collect all data, only segments of the signals where the dry electrode acquired ECG—which is susceptible to variations in contact pressure due to changes in skin-electrode-impedance³²—had a consistent amplitude were analyzed. Devices with both versions of the ECG featured a firmware modification which leveraged the lead-on detect feature of the ECG chip and would toggle a light-emitting diode facing the clinician between red and green for when ECG lead was detected as off or on, respectively. This also removed the possibility of accidentally applying an excessive amount of pressure without knowing whether a signal was being acquired.

In future work, though high-fidelity wearable measurements were acquired and only few minutes of data collection were necessary for this study, the wearable biosensor still needs further miniaturization to be used in future longitudinal studies in a pediatric population. However, given the considerably smaller footprint of the internal essential sensing elements, the hardware could readily be miniaturized and exploit the advent of flexible electronics which can offer a low-profile, less obtrusive solution for even greater convenience when performing longitudinal monitoring³³.

Signal processing and feature extraction

All signal processing and feature extraction was carried out in MATLAB 2018a (MathWorks, Natick, Massachusetts, USA) and entirely automated. A high-frequency SCG signal more closely related to the phonocardiogram was extracted for this analysis. The phonocardiogram, typically acquired from digital stethoscopes, is a wide bandwidth, high-frequency acoustic signal that captures heart sounds (i.e., S_1 and S_2) and obtains information of valve closures when placed at specific auscultation sites. Although, the phonocardiogram should be acquired using a wide-bandwidth, piezoelectric accelerometer (i.e., a contact microphone)

rather than the capacitive, direct current micro-electro-mechanical systems accelerometer used herein, the sampling rate of the accelerometer was increased to provide this bandwidth. First, the R-peaks of the ECG—marking ventricular depolarization—were found using Pan-Tompkins’s algorithm and used to determine the wearable HR. Then the SCG and high-frequency SCG signals were segmented into different heartbeats using and beginning with the detected R-peaks of the ECG. Due to the large differences in HR in this dataset, all of the heartbeats were zero-padded to a fixed length of 1300 ms, based on the slowest HR in the dataset. Next, the SCG and high-frequency SCG heartbeats were ensemble averaged using 30 heartbeat windows with 50% overlap—to reduce zero-mean noise, remove respiratory induced variability, and improve the consistency of amplitude features—before selecting the highest SNR beat—calculated using the algorithm in³⁴. First the envelope of the high-frequency SCG was computed which provided the profiles for the conventional heart sounds S_1 and S_2 . The algorithm for detecting the aortic opening point on the max SNR SCG beat was the same as that used in²⁰, where the aortic opening was detected by finding the nearest zero-crossing after the peak of the high-frequency SCG envelope between 0 and 150 ms; the aortic closing point was determined by finding the most consistent peak of the high-frequency SCG itself between 250 ms to the end of the beat. The aortic opening point resembles the PEP with the difference between that and the aortic closing point being the VET. Two other reciprocal features, PEP/VET and VET/PEP—systolic marker robust to differences in HR—are the quotient of the PEP and VET. Two interpretable systolic amplitude features were calculated as the RMS amplitude of the SCG during the PEP and during the VET. In total 9 systolic features were extracted from the wearable signals. Note that the HR from the CMR was added as a feature, due to both the inability to acquire continuous measurements with the wearable patch during the CMR—because of magnetic interference and injury— and due to expected high

accuracy in HR estimation when using wearable ECG during baseline measurements, as a closer measure of the HR during the reference measurement.

Leveraging surrounding physiological information can contextualize and improve the estimation accuracy of wearable measurements. The SV measurement from the CMR, is computed from a composition of several images which are obtained at a relatively slow sampling rate. Therefore, due to respiratory induced variability in SV readings—stemming from changes in venous return, preload, and HR—clinicians typically ask patients to hold their breath. However, as imaginable, for younger children this is obviously not possible. Instead, multiple scans are taken, and the resulting images are averaged before computing SV from the averaged image. Similarly, when using wearable measurements to accurately estimate SV compared to CMR readings should also factor in respiratory variability by averaging over a larger timespan—such as the 30 heartbeats employed in this analysis.

Machine learning

All machine learning and cross validation was performed in Python 3.0 using scikit-learn ridge regression and grid search packages, respectively. Despite a considerable sample size with respect to other SCG literature—especially given the diversity of demographics and diagnoses in such a diseased population—due to a small number of overall datapoints for a machine learning problem, multi-variate ridge regression was chosen as a less complex linear, and more interpretable, model to estimate SV³⁵. Ridge regression is similar to multiple-linear regression but with a regularization penalty—commonly referred to as lambda—that penalizes the model to prevent overfitting to the training data, thereby hopefully improving model generalizability³⁵.

10-fold cross validation was chosen as a commonly regarded robust method for optimizing hyperparameters and given that each subject had only one datapoint there would be

no overlap of subject-specific data in each fold. The completely randomized, held-out test set was determined by utilizing a true random number generator (RANDOM.ORG, Dublin, Ireland). To approximately balance and have a representative number of the number of single-ventricle patients in the training and testing set based on their size, originally during the data collection we again randomly split them into groups of four and three, respectively. However, after the final data was collected, a last single-ventricle patient was added to the training set to achieve a perfect 80%-20% split, hence a slight imbalance.

When selecting features for biomedical machine learning problem with a small dataset size there is a greater importance placed on not only selecting a few features that can explain a lot of the variance but also ones that can be clinically understood. Therefore, the original feature set of predictor variables consisted of 14 features that were chosen based on those with strong overlap between commonly used SCG features in existing literature and those that are simple and intuitive to cardiologists. Using forward feature selection on the training set, we decreased the feature set from 14 down to nine features based on the simple linear regression coefficient of determination between ECG and SCG features and SV. The Pearson's correlation coefficient values between these final nine features and SV, for the training set, are shown in Table S1.

We compared different ridge regression models trained on unique feature sets in our work. Specifically, we sought to compare models leveraging different combinations of ECG, SCG, and demographic (i.e., age and body surface area) features. Both training and testing set features were normalized based on the training set mean and standard deviation. The hyperparameter lambda for the highest performing model, which combined ECG and SCG features, came out to the maximum regularization penalty of 1.0.

Table S1. Training Set Correlation Coefficients Between Physiological Features and Stroke Volume.

Physiological Feature	Training Set Pearson's <i>r</i>
HR_{CMR}	-0.65
HR_{Wearable}	-0.63
VET	0.39
PEP	-0.02
PEP/VET	0.01
VET/PEP	-0.06
AC	0.45
RMS_{PEP}	-0.20
RMS_{VET}	-0.21

HR indicates heart rate; CMR, cardiac magnetic resonance imaging; VET, ventricular ejection time; PEP, pre-ejection period; AC, timing of aortic valve closure; RMS, root-mean-square power.

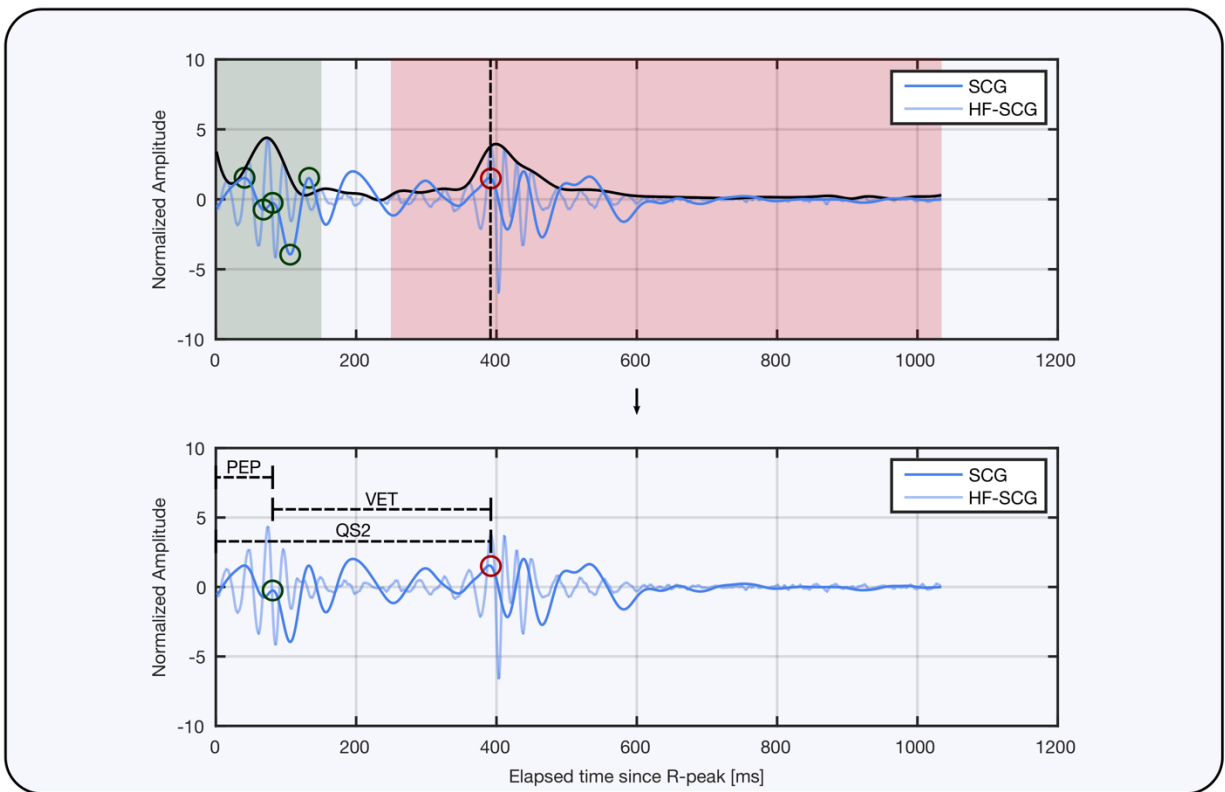
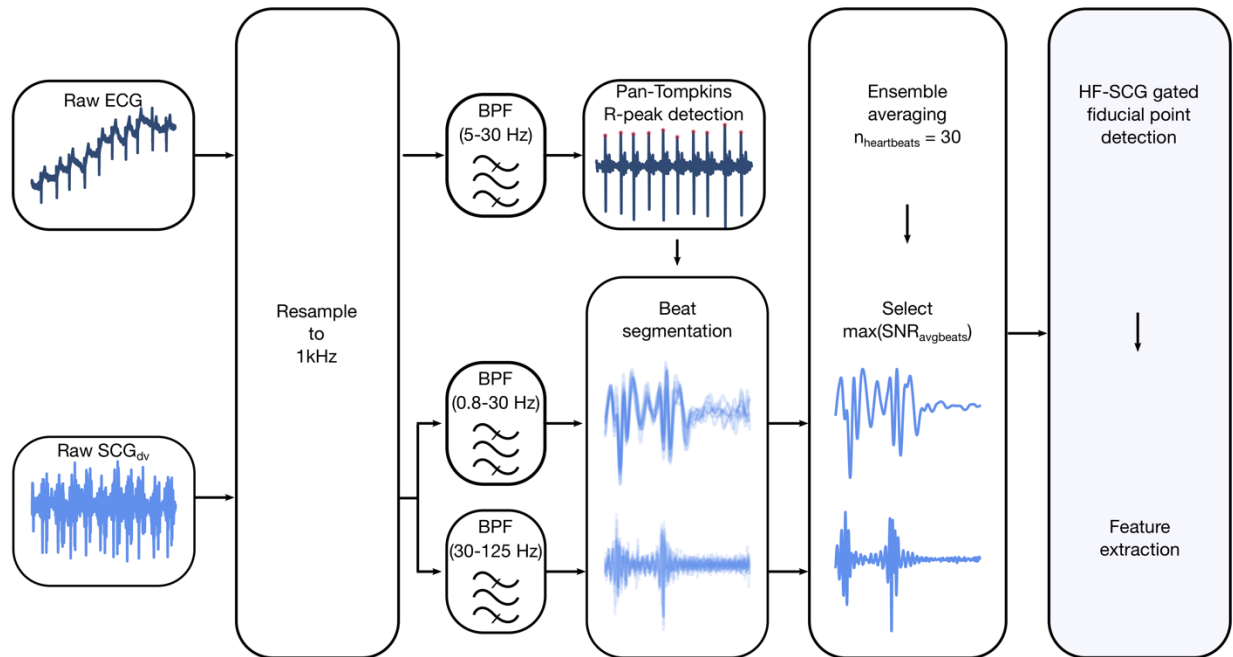


Figure S1. Signal processing pipeline. Block diagram of signal processing overview showing interpolation of electrocardiogram (ECG) and seismocardiogram (SCG) signals acquired from the wearable before bandpass filtering, R-peak detection, heartbeat windowing, and signal

quality assessment using the signal-to-noise ratio (SNR). Illustration of the custom high-frequency SCG (HF-SCG)—indicative of valve closures—assisted feature selection algorithm, helping to locate key fiducial points such as the aortic valve opening (AO) and aortic valve closure (AC) on the SCG—used to compute the pre-ejection period (PEP), ventricular ejection time (VET), and the AC. Additionally, the search radius for the AO (green) and AC (red) algorithm as well as their candidate points are shown.

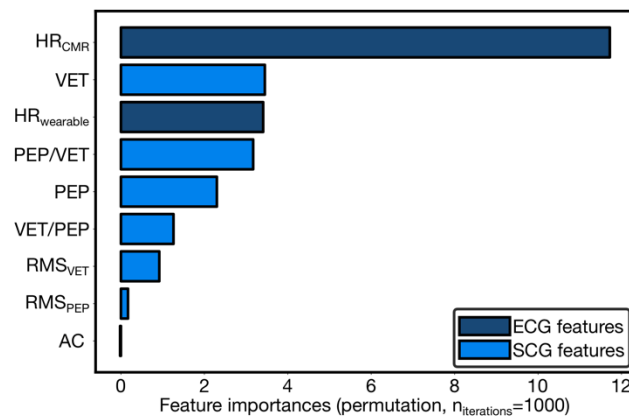


Figure S2. Permutation feature importances for stroke volume (SV) estimation model.

Permutation feature importances for wearable system with features randomly shuffled 1000 times, ranked in order from top to bottom, and color-coded by wearable sensing modality—electrocardiogram (ECG) and seismocardiogram (SCG) signals.